Evolution of supercurrent path in Nb/Ru/Sr$_2$RuO$_4$ dc-SQUIDs

Y. Nago,[1] R. Ishiguro,[2] T. Sakurai,[1] M. Yakabe,[1] T. Nakamura,[3] S. Yonezawa,[4] S. Kashiwaya,[5] H. Takayanagi,[1,6] and Y. Maeno[4]

[1]*Department of Applied Physics, Faculty of Science, Tokyo University of Science, Tokyo 125-8585, Japan*

[2]*Department of Mathematical and Physical Sciences, Faculty of Science, Japan Women's University, Tokyo 112-8681, Japan*

[3]*Institute of Solid State Physics, The University of Tokyo, Kashiwa, Chiba 277-8581, Japan*

[4]*Department of Physics, Graduate School of Science, Kyoto University, Kyoto 606-8502, Japan*

[5]*National Institute of Advanced Industrial Science and Technology, Tsukuba, Ibaraki 305-8568, Japan*

[6]*International Center for Materials Nanoarchitectonics, National Institute for Materials Science, Tsukuba, Ibaraki 305-0044, Japan*

Phase-sensitive measurements of direct-current superconducting quantum interference devices (dc-SQUIDs) composed of Sr$_2$RuO$_4$-Ru eutectic crystals have been performed to temperatures below a bulk Ru superconducting transition temperature at 0.49 K. A SQUID with Nb/Ru/Sr$_2$RuO$_4$ junctions fabricated on one Ru inclusion exhibits two distinct transitions due to the Ru superconducting transition and competition of proximity-induced superconducting gaps at the junctions. At sufficiently low temperatures, the SQUID interference patterns start to collapse with large phase shifts of the Fraunhofer patterns. This result indicates the influence of magnetic fluxes induced by large bias currents flowing in a strongly asymmetric supercurrent path. Such a large change in supercurrent path suggests superconducting phase mismatch between the *s*-wave and chiral *p*-wave states at the Ru/Sr$_2$RuO$_4$ interface.

I. INTRODUCTION

The layered perovskite Sr$_2$RuO$_4$ has been attracting much research interest because it is one of the strong candidates of a spin-triplet chiral *p*-wave superconductor [1–3]. Nuclear magnetic resonance (NMR) [4,5], muon spin rotation (μSR) [6], and Kerr-effect measurements [7] have established an equal-spin triplet-pairing state with broken time-reversal symmetry. These results propose a chiral *p*-wave state of orbital wave function represented by $k_x \pm i k_y$. A Sr$_2$RuO$_4$-Ru eutectic crystal is also an interesting material because it exhibits an inhomogeneous superconducting phase below 3 K (the 3-K phase), different from the bulk phase which appears at 1.5 K [8]; the 3-K phase is expected to nucleate as a single-component paring state k_x conserving time-reversal symmetry at the interface with Ru inclusion and evolves into a state breaking time-reversal symmetry with decreasing temperature [9]. Therefore this eutectic is helpful to understand superconductivity of Sr$_2$RuO$_4$. Indeed, there are some reports in both single and eutectic crystals supporting the chiral *p* pairing symmetry, such as the observation of the Andreev bound state [10–12], anomalous behavior attributable to chiral domains [13–15], and the anomalous Josephson network [16]. However, the typical size of a chiral domain and the presence of a spontaneous edge current have still been open questions [17–19].

Josephson junctions provide a powerful means to investigate the pairing symmetry of a superconductor [20] because the Josephson coupling of the junction composed of an unconventional superconductor is dependent on the junction orientation: in the case of a singlet/triplet superconducting junction, the lowest-order Josephson current density J_s flowing through the superconductors with an order parameter of ψ_s for a spin-singlet state and $\bm{d}(\bm{k})$ for a spin-triplet state is expressed by [21–26]

$$J_s \sim \langle \psi_s (\bm{k} \times \bm{n}) \cdot \bm{d}(\bm{k}) \rangle_{FS}, \qquad (1)$$

where $\bm{k}$ is the wave number, $\bm{n}$ is the interface normal vector, and angle brackets with a subscript FS denote the average over the Fermi surface. The Josephson effect at a single junction using Sr$_2$RuO$_4$ and different *s*-wave superconductors has been investigated for over a decade [13,27–29]. Jin *et al.* and Liu *et al.* confirmed the selection rule in the junction orientation dependence, consistent with Eq. (1) [25], and the novel temperature dependence of the Josephson critical current [30], which was interpreted by the theory assuming the *p*-wave pairing symmetry of Sr$_2$RuO$_4$ [31,32].

Sr$_2$RuO$_4$-Ru eutectic crystals are useful for fabricating a *topological superconducting junction* [15,33] because Ru inclusions naturally created in bulk Sr$_2$RuO$_4$ provide very clean Ru/Sr$_2$RuO$_4$ interfaces and are good for contact with other metals via Ru. The eutectic crystal also enables us to investigate a competition between the *s*-wave state of Ru and the chiral *p*-wave state of Sr$_2$RuO$_4$ below the superconducting transition temperature T_c^{Ru} of a Ru inclusion (0.49 K). A topological mismatch between both phases is expected to cause Josephson vortex nucleation in a Ru inclusion [34]: a frustrating coupling of the order parameters between the *s*- and *p*-wave superconductivities induces a spontaneous magnetic flux distribution at the interface of Ru inclusion, increasing with decreasing temperature to form a single vortex at the Ru center. Maeno *et al.* fabricated the superconducting/normal/superconducting (S/N/S) topological superconducting junction using the eutectic, revealing anomalous features of the Josephson current due to a competition between the *s*-wave state and the chiral *p*-wave state [15,33]. The mechanism of the anomalous temperature dependence of the Josephson critical current has recently been discussed using the theoretical model based on the spontaneously induced magnetic flux [35,36]. However, unambiguous evidence of the spontaneous vortex nucleation in Ru has not been obtained experimentally. Also, systematic experiments have not been performed at temperatures lower than T_c^{Ru} except for tunneling spectroscopy measurements, which revealed suppression of a *p*-wave gap in Ru inclusions [37].

A tunneling measurement with a single lateral junction is not necessarily sufficient to study the pairing symmetry because it is sensitive mainly to the magnitude of the superconducting gap. Phase-sensitive measurements using superconducting quantum interference devices (SQUIDs) are one of the effective devices to determine k dependence of the order parameter of Sr_2RuO_4 [20,22,26]. In fact, such SQUID experiments using Sr_2RuO_4 and an s-wave superconductor revealed the odd-parity pairing symmetry with π-phase change [38]. This is consistent with Eq. (1), providing strong support for the p-wave pairing state. Clarification of superconductivity at the s-wave/chiral-p-wave superconducting junction requires more profound phase-sensitive measurements using SQUIDs. We have so far fabricated dc-SQUIDs with Nb/Ru/Sr_2RuO_4 junctions using Sr_2RuO_4-Ru eutectic crystals [39] and measured their transport properties [40]. In these studies, the SQUID loops were made with two separate Ru inclusions. In contrast, in the present device we used a single Ru inclusion to form the SQUID loop. In this way, the SQUID loop is made purely with s-wave superconductors, Nb and Ru, below 0.5 K, and the loop is connected to Sr_2RuO_4 surrounding the Ru inclusion. Such a configuration is expected to maximize the phase competition between the s-wave and p-wave superconductivities as the device forms the *topological junction* [33]. In this study, we investigate detailed properties of the junction introduced in Ref. [41]. In particular, we reveal an anomalous shift of the Fraunhofer interference patterns attributable to phase competition between superconductivities in Ru and Sr_2RuO_4.

II. EXPERIMENT

As shown in Fig. 1, the dc-SQUIDs used in this study consist of Nb, Sr_2RuO_4, and two Nb/Ru/Sr_2RuO_4 junctions on the ab-plane surface of a Sr_2RuO_4-Ru eutectic crystal, cut from a crystalline rod grown with a floating-zone method [8]. The device was fabricated with the same technique used in previous studies [39,40]: the eutectic crystal is coated with a SiO_2 layer 300 nm thick, and two small holes are made directly above a selected Ru inclusion for contacting a niobium electrode using photolithography and a reactive ion etching. The structure of the present device is similar to the one in previous studies [39,40], except that the two junctions are made on each edge of the *same* Ru inclusion, as shown in Figs. 1(a) and 1(b). The area of the Ru inclusion on the surface is about $1 \times 21\,\mu$m. The effective junction width w, defined as the sum of the inner separation of the Nb posts and the width of one post, is 20.9 μm [Figs. 1(b) and 1(c)]. A SQUID loop should be formed so that a bias current flows into Sr_2RuO_4 in the vicinity of the Ru/Sr_2RuO_4 interface, for example, as indicated by the red line in Fig. 1(a). At temperatures below around T_c of the 3-K phase down to T_c^{Ru}, the Ru inclusion is in a weak superconducting state due to the proximity effect of the superconducting Nb, realizing Nb (S)/Ru (N)/Sr_2RuO_4 (S) weak-link Josephson junctions. When Ru undergoes a superconducting transition at T_c^{Ru}, the junction structure changes from S/N/S to S/S/S. A competition between the s-wave superconductivity of Ru and the unconventional superconductivity of Sr_2RuO_4 is expected to affect junction properties of the SQUID.
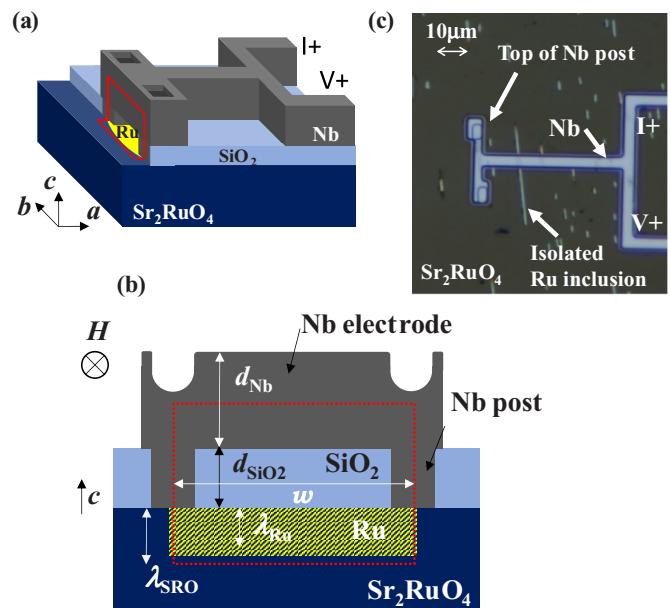
FIG. 1. (a) Configuration of a dc-SQUID with Nb/Ru/Sr_2RuO_4 junctions. Two junctions are located on the same Ru inclusion. The red line indicates an expected SQUID loop. (b) Schematic of the SQUID. The effective width w is 20.9 μm. d_{Nb} and d_{SiO2} indicate the thickness of the Nb electrode (0.6 μm) and SiO_2 (0.3 μm), respectively. (c) Photograph showing the top view of the SQUID after sputtering niobium electrodes. Other Ru inclusions isolated from the Nb electrodes by the SiO_2 layer can also be seen.

For four-terminal measurements, two Nb electrodes (I+ and V+) with a thickness of $d_{Nb} = 0.6\,\mu$m are directly linked to the SQUID as shown in Fig. 1, and the other two (I− and V−) are deposited on two other separate Ru inclusions [see Fig. 1(a) in Ref. [39]]. The device was placed in a dilution refrigerator or a ^{3}He refrigerator and cooled down below 1 K. In the temperature range below 0.5 K, a considerably large current up to an order of a milliampere needs to be applied in order to measure a maximum Josephson current I_c [41]. Thus heat generated by the current at the junctions and in the electrical wires made of a normal metal connected to the device is an inevitable problem. In fact, during the repetition of the measurements of the IV characteristics at each controlled temperature, we found a gradual decrease of I_c due to heating. In order to minimize such a heating effect, we set a wait time of 5 to 15 min between each measurement, depending on temperature.

III. RESULTS AND DISCUSSION

In the following, we describe the results and interpretations featuring three temperature ranges: above T_c of Ru (Sec. III A), just below T_c of Ru (Sec. III B), and below 0.40 K, where peculiar interference is observed (Sec. III C).

A. SQUID interference patterns and SQUID zero-peak shifts

Figure 2(a) shows the maximum Josephson current I_c as a function of external magnetic field $\mu_0 H$ normal to the loop area at temperatures from 0.60 to 0.45 K, derived
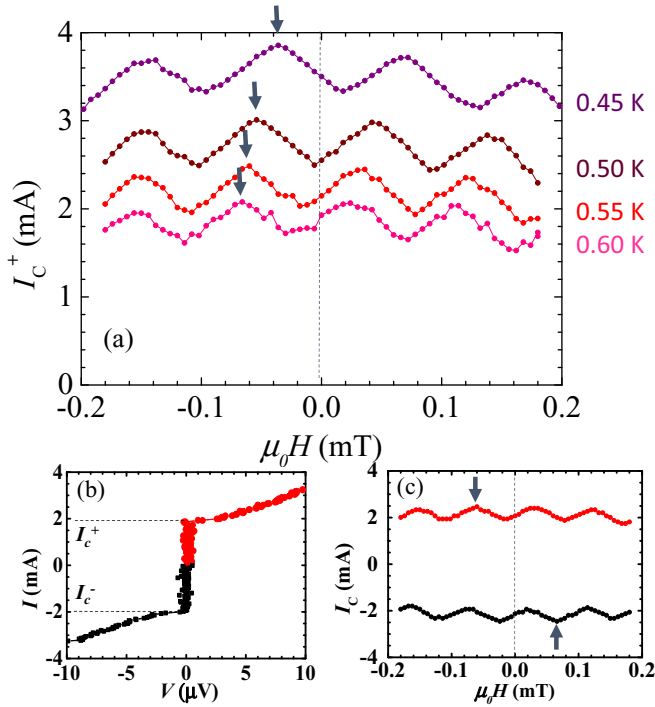
FIG. 2. (a) Maximum Josephson current as a function of external magnetic field $\mu_0 H$ in a temperature range of 0.45–0.60 K. (b) Current-voltage characteristics of the SQUID at 0.55 K and zero magnetic field. Maximum Josephson current I_c is determined for both current directions, as indicated by I_c^+ and I_c^-, at which the voltage exceeds $\sim 1\mu$V. (c) I_c^+ and I_c^- as a function of external magnetic field at 0.55 K. Arrows indicate the SQUID zero-peak shifts. The zero peaks are located at symmetric positions.

from *IV* characteristics [Fig. 2(b)]. Here μ_0 represents the vacuum magnetic permeability. I_c exhibits periodic SQUID-interference patterns superposed on a broad envelope of a Fraunhofer diffraction pattern, as observed in previous studies [41]. This underlining Fraunhofer envelope originates from the flux penetration in the junction area below each Nb post. The period ΔB_{SQ} of the SQUID-interference patterns is approximately 0.09 mT at 0.55 K. This corresponds to the flux quantum Φ_0 (=2.07×10^{-15} Wb) divided by the effective SQUID-loop area A_{eff}. In our device, a supercurrent flows from a Nb lead to surfaces of the bulk Sr$_2$RuO$_4$ (more precisely, "near" surfaces because *p*-wave pair function is considered to be suppressed at the top *ab* surface [25,42]) through the Nb/Ru/Sr$_2$RuO$_4$ junction, as indicated by the red loop in Figs. 1(a) and 1(b). The depth of the Ru inclusion is expected to be on the order of a micron or more [8]. However, it is anticipated that what contributes to the effective SQUID-loop area A_{eff} is the penetration depth of magnetic flux into Sr$_2$RuO$_4$ (λ_{SRO}) rather than the depth of the Ru inclusion. This is because the Ru inclusion is fully surrounded by superconducting Sr$_2$RuO$_4$ [Fig. 1(a)], which screens the external field. Therefore the effective SQUID-loop area is expressed by $A_{eff}(T) \sim w[d_{Nb}/2 + d_{SiO2} + \lambda_{SRO}(T)]$, where the effective junction width is $w = 20.9\,\mu$m, the thickness of the Nb electrode $d_{Nb} = 0.6\mu$m, and the thickness of the SiO$_2$ $d_{SiO2} = 0.3\,\mu$m [Fig. 1(b)]. Consequently, a SQUID period

ΔB_{SQ} is represented by

$$\Delta B_{SQ} = \frac{\Phi_0}{A_{eff}(T)}$$

$$\cong \frac{\Phi_0}{w[d_{Nb}/2 + d_{SiO2} + \lambda_{SRO}(T)]}. \quad (2)$$

The period $\Delta B_{SQ} = 0.09$ mT at 0.55 K leads to $\lambda_{SRO}(T = 0.55$ K$) \sim 0.50\,\mu$m from Eq. (2). If the external field H is parallel to the *ab* plane of the eutectic as in Fig. 1(b), λ_{SRO} should be the penetration depth along the *c* axis of Sr$_2$RuO$_4$ ($\sim 3\,\mu$m) [3]. However, the estimated magnitude of $\lambda_{SRO}(T = 0.55$ K$)$ is rather close to the penetration depth along the *ab* plane ($\sim 0.1\,\mu$m) [43]. It can be attributed to the alignment deviation of the eutectic crystal against the direction of the applied field.

The I_c^+ vs $\mu_0 H$ patterns in Fig. 2 exhibit a nonsinusoidal modulation. In the case of the SQUID with the screening parameter $\beta_L \equiv 2LI_c/\Phi_0 > 1$, where L is a loop inductance, magnetic fluxes induced by the bias current influence the modulation pattern. The critical current modulation amplitude is deduced to be $\Delta I_c/I_c \sim 0.17$ at 0.5 K from Fig. 2. Therefore the screening parameter is estimated to be $\beta_L = I_c/\Delta I_c - 1 = 4.9$ [44–46], which is large enough to cause the nonsinusoidal I_c vs $\mu_0 H$ pattern seen in Fig. 2. The estimated value of β_L leads to the inductance $L \sim 1.7$ pH. This inductance is equivalent to a square SQUID loop with the inner side length $a = L/\mu_0 \sim 1\,\mu$m, consistent with the micron-sized SQUID shown in Fig. 1.

It should be noted that the above discussion about β_L is just a rough maximum estimate; the present SQUID does not consist of tunnel junctions (but S/N/S) and is not completely symmetric ($L^{left} \neq L^{right}$, $I_c^{left} \neq I_c^{right}$). These features also influence the I_c modulation. For the former, a phase slip of the superconducting order parameter influences the phase-current relation at the junctions [47]. For the latter, an asymmetry of the junctions influences the modulation amplitude and the phase offset of the SQUID pattern [44]. In fact, the field at which I_c^+ takes a maximal value, as shown by arrows in Fig. 2(a), is shifted to the negative direction from $\mu_0 H = 0$ mT. Similarly, the field with the maximal $|I_c^-|$ in Fig. 2(b) is also shifted by almost the same amount but to the positive field direction, as shown in Fig. 2(c). This offset (SQUID "zero-peak" shift) indicates the presence of the asymmetry of the device structure.

Unconventional superconductivity of Sr$_2$RuO$_4$ can also contribute to the I_c vs $\mu_0 H$ modulation patterns. The current-phase relation of the Josephson current is generally given by

$$I_s(\phi) = \sum_n [I_{an}\sin(n\phi) + I_{bn}\cos(n\phi)], \quad (3)$$

where ϕ indicates phase difference between the junctions. When the superconducting order parameter conserves time-reversal symmetry, I_{bn} vanishes, and $I_{a1}\sin(\phi)$ is dominant ($I_{a1} = I_c$). In contrast, the present SQUID junctions include superconducting Sr$_2$RuO$_4$ with a broken time-reversal symmetry ($k_x + ik_y$), and hence it is possible that $I_{a1} = 0$ and the contribution of other terms in Eq. (3) becomes dominant [22,23]. Such a SQUID exhibits a nonsinusoidal I_c modulation.

For a SQUID based on Sr$_2$RuO$_4$, the maximum Josephson current at the external field $\mu_0 H = 0$ mT depends on the
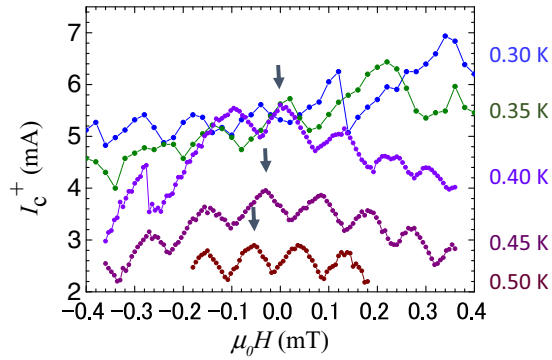
FIG. 3. Maximum Josephson current as a function of external magnetic field within a temperature range of 0.30–0.50 K. Arrows indicate the SQUID zero-peak shifts.

orientation between the two junctions on the *ab* plane [26] because a chiral-*p* state of Sr_2RuO_4 shows a phase winding in the momentum space ($k_x + ik_y$). Actually, a previous SQUID experiment [38] indicates that the symmetric SQUID with junctions fabricated on opposite sides of a bulk Sr_2RuO_4 exhibits π-SQUID behavior. Although our present SQUID has Nb/Ru interfaces positioned on the same *ab* surface of the eutectic, in the present SQUID geometry it is plausible that a supercurrent will flow through the Ru/Sr_2RuO_4 interface positioned perpendicular to the *ab* face [$n \perp c$ axis $\parallel d$, see Eq. (1)] so that the current path makes the shortest loop, as depicted in Fig. 1(a). Our results, exhibiting almost no phase shifts of the interference patterns except for the influence by self-induced flux, indicate that both junctions orient in the same direction at the Ru/Sr_2RuO_4 interfaces.

B. SQUID patterns with Ru in the superconducting state

Figure 3 shows the temperature dependence of SQUID interference patterns at temperatures lower than 0.50 K. The responses of SQUID interference patterns reveal two distinct transition temperatures, as shown in Figs. 4 and 5 [41]. One
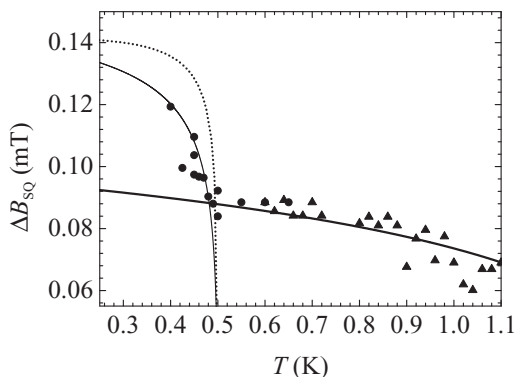
FIG. 4. Temperature dependence of the SQUID period ΔB_{SQ}. Solid circles and triangles represent data obtained with different cryostats. The thick solid curve shows the fitting line at temperatures higher than 0.50 K, estimated from Eq. (2) with a penetration depth of Eq. (4), in which T_c of Sr_2RuO_4 is chosen to be 1.5 K. Dotted and thin solid curves show the period estimated from the London penetration depth of Ru with $T_c^{Ru} = 0.50$ K (see text).
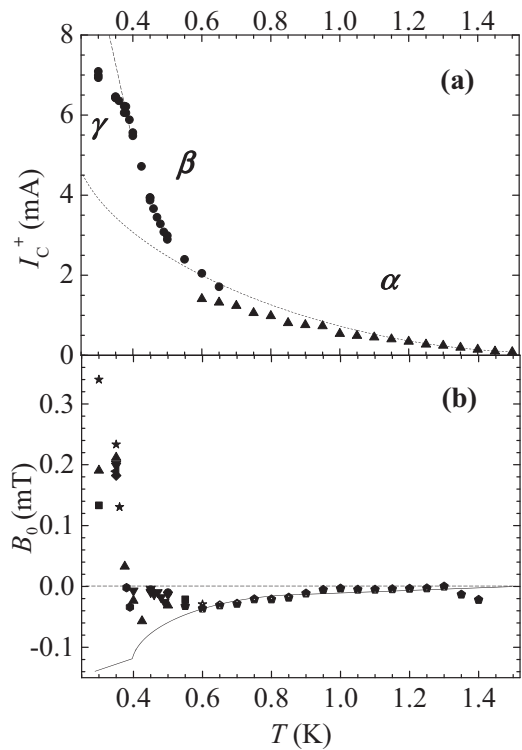
FIG. 5. (a) Temperature dependence of maximum value in I_c^+ modulation seen in Figs. 2 and 3. Different symbols indicate data obtained using different cryostats. (b) Fraunhofer zero-peak shift B_0 as a function of temperature. Below 0.40 K, $I_c^+(T)$ behavior changes, and B_0 shows a sign change as well as the enhanced magnitude. Different solid symbols indicate the data obtained during different cooling cycles, and the solid curve is based on the estimated values from the data in (a) (see text).

is about 0.50 K, where the SQUID period ΔB_{SQ} exhibits a sharp increase. The other is about 0.40 K, below which the SQUID pattern starts to collapse. This latter behavior will be described in Sec. III C. The SQUID I_c exhibits interference behavior below about 1.45 K, and ΔB_{SQ} gradually increases with decreasing temperature down to 0.50 K, as seen in Fig. 4. According to Eq. (2), the increase of ΔB_{SQ} is attributable to a gradual decrease of the penetration depth of Sr_2RuO_4 $\lambda_{SRO}(T)$. The temperature dependence of ΔB_{SQ} is well described by Eq. (2), assuming $\lambda_{SRO}(T)$ to be

$$\lambda(T) = \lambda_L \left(1 - \frac{T}{T_c} \right)^{-\frac{1}{2}} \tag{4}$$

for the case of $\lambda(T) > \xi_0$ near T_c [48]. Here λ_L indicates the London penetration depth, and ξ_0 indicates the coherence length. The thick solid curve in Fig. 4 indicates the period estimated from Eq. (2) using Eq. (4), in which T_c for Sr_2RuO_4 is chosen to be 1.5 K. This curve fits well our data with a fitting parameter λ_L of 0.43 μm.

Below 0.50 K, however, one can see an abrupt increase of ΔB_{SQ}. The increase of the period indicates a decrease of the effective SQUID-loop area A_{eff}. When the Ru inclusion undergoes a superconducting transition, the Meissner screening in the superconducting Ru area leads to a decrease of A_{eff}. Since the temperature dependence of $\lambda_{SRO}(T)$ is weak
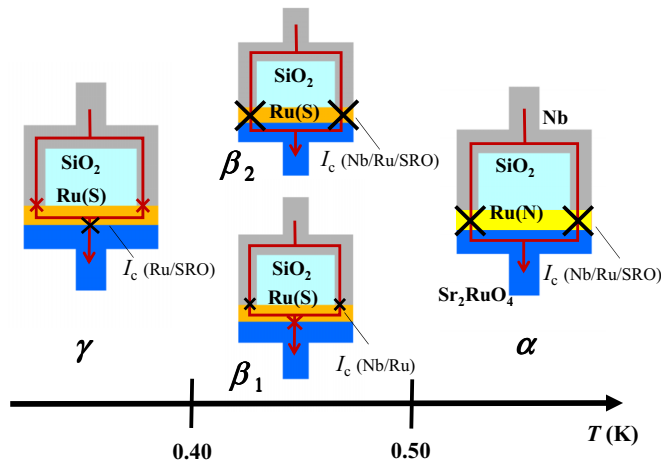
FIG. 6. Possible supercurrent paths in the device in the different temperature ranges corresponding to α, β, and γ indicated in Fig. 5. In α, the SQUID loop consists of S/N/S junctions shown by black crosses. In β, there are two possible supercurrent paths: β_1, where the SQUID loop contains a superconducting Ru path and I_c is limited by the Nb/Ru junctions (black crosses), rather than the Ru/Sr$_2$RuO$_4$ (SRO) junction (red cross), and β_2, where the current path is essentially the same as in α but the SQUID loop consists of S/S/S junctions shown by black crosses. In γ, the SQUID loop is essentially the same as in β_1, but I_c is limited by the Ru/SRO junction (black cross).

at sufficiently low temperatures, it is expected that $\lambda_{\mathrm{SRO}}(T)$ in Eq. (2) is replaced by a penetration depth of Ru $\lambda_{\mathrm{Ru}}(T)$ [Fig. 1(b)]. Therefore the effective loop area is expressed by $A'_{\mathrm{eff}}(T) \sim w[d_{\mathrm{Nb}}/2 + d_{\mathrm{SiO2}} + \lambda_{\mathrm{Ru}}(T)]$. The dotted curve in Fig. 4 indicates the period estimated from the form $\lambda(T)/\lambda_L = [1 - (T/T_c)^4]^{-1/2}$ by the London theory in which λ_L and T_c for Ru are assumed to be $\sim 0.1\,\mu$m and 0.50 K, respectively. The thin solid curve shows the period estimated by Eq. (4). This expression seems to be a better fit to our data. Although the penetration depth of the Ru inclusion might not be completely described by the London theory, these results confirm that the observed abrupt increase of ΔB_{SQ} indicates the reduction of the effective SQUID-loop area due to the superconducting transition of the Ru inclusion at $T_c^{\mathrm{Ru}} = 0.50$ K.

Below T_c^{Ru}, a superconducting path through the Ru inclusion newly appears, and a supercurrent flows through the whole Ru inclusion; that is, the SQUID structure changes from α to β_1 in Fig. 6. Strictly speaking, the amplitude of the pair function of the superconducting Ru ψ_s^{Ru} is still weak just below $T_c^{\mathrm{Ru}} = 0.50$ K, and hence the device might maintain the supercurrent path α, i.e., a Nb/Ru/Sr$_2$RuO$_4$ (S/S/S) SQUID (β_2 in Fig. 6), even below T_c^{Ru} [41]. In this case, as ψ_s^{Ru} is gradually enhanced with decreasing temperature, the transition from path β_2 to path β_1 occurs at a temperature somewhat below T_c^{Ru}.

The maximum Josephson current I_c gradually increases with decreasing temperature down to T_c^{Ru}, as seen in Fig. 5(a). This increase is attributable to a temperature dependence of the superconducting gap of Sr$_2$RuO$_4$ at the junction. Although I_c does not exhibit any abrupt increase below T_c^{Ru}, it clearly shows an excess increase. This indicates reinforcement of a coupling of proximity-induced pair functions at the junction.

Below T_c^{Ru}, circuit β_1 or β_2 in Fig. 6 is formed. In the case of β_1, the circuit consists of a series circuit with a superconducting ring with Nb/Ru junctions and a single Ru/Sr$_2$RuO$_4$ junction. In this case, between two relevant critical currents, I_c of the Nb/Ru junctions (SQUID) and I_c of the Ru/Sr$_2$RuO$_4$ junction, the smaller one is what is observed. Figure 3 shows that the SQUID maintains its periodic modulation of I_c even just below T_c^{Ru}. Therefore it is the Nb/Ru SQUID junctions which limit the circuit I_c at this temperature range. On the other hand, in the case of β_2, the device maintains the SQUID with Nb/Ru/Sr$_2$RuO$_4$ (S/S/S) junctions, consistent with the present results. In any case, creation of the Cooper pairs of a Ru superconducting state reinforces a coupling with the pair function of the superconducting Nb or Sr$_2$RuO$_4$ at the junction, resulting in the excess increase of I_c^+ in Fig. 5(a).

In addition to the shift of the SQUID zero peak shown in Figs. 2 and 3, the underlining Fraunhofer pattern also shows a peak shift B_0. Here the Fraunhofer zero-peak shift B_0 is deduced from the envelope of the oscillating $I_c(H)$ [Fig. 2(a)]. Down to 0.60 K, B_0 shifts in the negative direction with decreasing temperature, as seen in Fig. 5(b) [49]. B_0 is almost symmetric between I_c^+ and I_c^-, indicating the magnetic flux induced by the bias current affects the field shift. This self-field shift depends on the self-inductance per unit area l_s of the device and the maximum Josephson current I_c, i.e., $B_0 = l_s I_c$. The solid curve in Fig. 5(b) shows the self-field shifts estimated from I_c^+ in Fig. 5(a), assuming l_s is constant at 0.02 H/m^2, which is obtained from B_0/I_c^+ at 0.8 K. The experimental data B_0 at high temperatures are in good agreement with the estimated values; however, the magnitude of B_0 decreases below around T_c^{Ru}, deviating from the estimated values. This indicates that l_s decreases with decreasing temperature. It is possible that, at temperatures from 0.50 down to 0.40 K, the current path through the device gradually changes from β_2 to β_1 in Fig. 6, depending on temperature.

C. Collapse of the SQUID pattern below 0.40 K

The second transition is unexpectedly observed at 0.40 K, below which the temperature dependence of I_c changes quantitatively, as seen in Fig. 5(a). Concurrently, the SQUID interference pattern starts to collapse along with large shifts of the zero-peak B_0, which is clear in Fig. 3. It is surprising that the sign of B_0 reverses at 0.40 K, and its magnitude below 0.40 K depends on the cooling cycle, as seen in Fig. 5(b); when the device was warmed up to above T_c^{Ru} and then cooled again, the magnitude of B_0 was not always reproducible. Such anomalous characteristics were not observed for the previous SQUID with two junctions connected to two different Ru inclusions [39,40].

The anomalous increase of B_0 suggests the presence of magnetic fluxes in the junction at zero field, such as a vortex trapped in defects or impurities in a superconductor [50] or a flux induced by a bias current due to the asymmetric structure of the device [48]. Our results revealed no significant hysteresis, as shown in Fig. 7, and the zero-peak shift B_0 is almost symmetric between I_c^+ and I_c^-, as seen in the inset of Fig. 7. These characteristics are not consistent with those due to a trapped vortex. The B_0 symmetry indicates that the large B_0 observed below 0.40 K is caused by self-induced magnetic
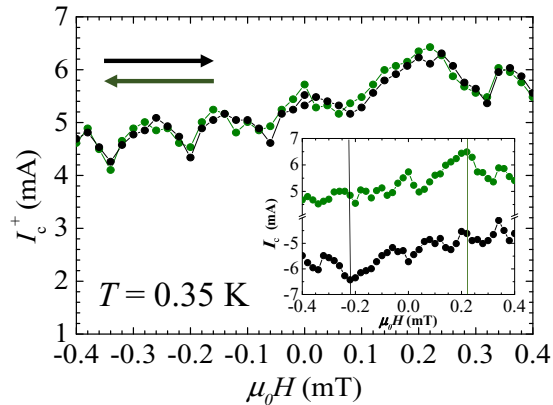
FIG. 7. Modulation of I_c^+ with up and down sweeps of external magnetic field at 0.35 K. The inset indicates the up-sweep data of I_c^+ and I_c^-. Vertical solid lines show the field value at the Fraunhofer zero peak. The shifts in the zero peaks are in the symmetric positions.

fluxes. The supercurrent path through the device appears to change substantially below 0.40 K.

The change in I_c vs T and the collapse of the SQUID pattern suggest substantial a change in the junction property. If the SQUID junctions still contain Sr_2RuO_4 at 0.40 K, like β_2 in Fig. 6, it is possible that the collapse of the SQUID pattern could be attributed to a chiral p-wave state $k_x + ik_y$ of Sr_2RuO_4. If higher-order terms in Eq. (3) become more dominant with decreasing temperature, such a change in the current-phase relation at the junction might lead to a reduction of the modulation amplitude in the I_c vs μ_0H characteristics. This scenario supports the unconventional superconductivity of Sr_2RuO_4. However, it cannot explain the change in the supercurrent path to the extent that the magnitude of B_0 rapidly increases along with its sign change below 0.40 K, as in Fig. 5(b).

If the supercurrent path β_1 in Fig. 6 is formed at 0.40 K, there is no contribution of the superconductivity of Sr_2RuO_4 to the collapse of the SQUID pattern. In this case, the collapse of the SQUID pattern suggests that it is I_c of a single Ru/Sr_2RuO_4 junction that is observed below 0.40 K. It is plausible that as the amplitude of the pair function of Ru ψ_s^{Ru} is enhanced with decreasing temperature, I_c of Nb/Ru junctions becomes strong enough to exceed that of the single Ru/Sr_2RuO_4 junction; as for the latter, the rate of increase in I_c is expected to be small because of the phase mismatch between s- and chiral p-wave states. Thus the SQUID structure collapses as it changes from β_1 to γ in Fig. 6. In γ, the superconductivity of Sr_2RuO_4 (especially a topological junction) is expected to influence the junction property.

The poor reproducibility of B_0 in Fig. 5(b) implies the presence of multiple metastable current paths. Similar behavior in I_c was observed in the previous measurements at temperatures higher than T_c^{Ru} [15]. Anwar *et al.* [15] have discussed the influence of the motion of chiral-domain-walls pinned at the Ru/Sr_2RuO_4 interface. In our device, however, we did not obtain remarkable evidence of the domain-wall motion such as telegraphic noise in I_c or hysteresis in the I_c vs μ_0H characteristics. This fact implies a different mechanism.

We note in Fig. 5 that with decreasing temperature below 0.40 K, the self-field at the junction B_0 continues to increase rapidly, although I_c does not change substantially. We also note that the value of B_0 shows poor reproducibility among different cooling cycles. Such unusual behavior is ascribable to the phase competition between the s-wave Ru and chiral p-wave Sr_2RuO_4 in the path γ in Fig. 6. In our device, there is a phase winding of Sr_2RuO_4 around the Ru inclusion, which leads to frustration with the superconducting phase of the Ru. As the pair amplitude in the Ru gets stronger with decreasing temperature, the phase competition forces the supercurrent to flow in a different path, avoiding chiral domains and maximizing the critical current. Such a scenario can explain the unusual temperature evolution as well as poor reproducibility in B_0. Recent studies [34–36] show that the increase in the s-wave pair amplitude with decreasing temperature strengthens the Josephson coupling with p-wave states, resulting in the asymmetric spontaneous supercurrent profile at the Ru/Sr_2RuO_4 interface. It is possible that such a gradual change in the supercurrent profile induces the magnetic fluxes leading to the large self-field shift in I_c vs μ_0H characteristics as in Fig. 5(b).

A spontaneous supercurrent induced by the phase mismatch of s- and p-wave states at the Ru/Sr_2RuO_4 interface possibly leads to a vortex nucleation in Ru [34]. However, our present results show the absence of the vortex and only self-induced fluxes, as can be seen from Fig. 7. Different from the theoretical model [34], the Ru inclusion does not thread through the crystal in our device, and conceivably, the generation of a vortex in a Ru inclusion may not be energetically favorable. It is necessary to devise a simpler SQUID to investigate a spontaneous vortex nucleation. We have a technique to fabricate a Sr_2RuO_4 microsample using a focused ion beam and a magnetization measurement device using a micro dc-SQUID [51–53]. It is useful to detect the magnetic flux induced by a spontaneous vortex nucleation in a Ru inclusion of a eutectic crystal.

Although we discussed the mechanism of the anomalous interference based on the chiral p-wave symmetry of Sr_2RuO_4, the possibility of helical p-wave symmetry has also been pointed out as an alternative candidate recently [18]. Further experimental and theoretical approaches are required to clarify whether or not helical p-wave symmetry could also describe our present results.

IV. CONCLUSION

We fabricated a dc-SQUID with $Nb/Ru/Sr_2RuO_4$ junctions on one Ru inclusion of a Sr_2RuO_4-Ru eutectic crystal and investigated its magnetic interference patterns down to 0.3 K. The superconducting transition of the Ru inclusion and the balance of the proximity-induced superconductivity of each superconductor at the junction cause two transitions in the interference patterns due to evolution of the supercurrent path. At $T > 0.50$ K, the S/N/S-junction SQUID (α in Fig. 6) is realized, while at $T < 0.40$ K, path γ in Fig. 6 is formed. From 0.50 down to 0.40 K, it is possible that the path gradually changes from β_2 to β_1. The Ru/Sr_2RuO_4 single topological junction is formed at $T < 0.40$ K, and phase

competition between the chiral superconductivity of Sr_2RuO_4 and the s-wave superconductivity of Ru causes a change in supercurrent profiles at the Ru/Sr_2RuO_4 interface. This scenario provides a good interpretation of the collapse of the SQUID patterns with large phase shifts of the Fraunhofer patterns. Although there does not appear to be direct evidence of spontaneous vortex nucleation due to the phase competition, these experimental results support chiral superconductivity of Sr_2RuO_4. A SQUID is a very efficient tool to investigate unconventional superconductivity.

[1] Y. Maeno, H. Hashimoto, K. Yoshida, S. Nishizaki, T. Fujita, J. G. Bednorz, and F. Lichtenberg, Nature (London) **372**, 532 (1994).

[2] A. P. Mackenzie and Y. Maeno, Rev. Mod. Phys. **75**, 657 (2003).

[3] Y. Maeno, S. Kittaka, T. Nomura, S. Yonezawa, and K. Ishida, J. Phys. Soc. Jpn. **81**, 011009 (2012).

[4] K. Ishida, H. Mukuda, Y. Kitaoka, K. Asayama, Z. Q. Mao, Y. Mori, and Y. Maeno, Nature (London) **396**, 658 (1998).

[5] K. Ishida, M. Manago, T. Yamanaka, H. Fukazawa, Z. Q. Mao, Y. Maeno, and K. Miyake, Phys. Rev. B **92**, 100502 (2015).

[6] G. M. Luke, Y. Fudamoto, K. M. Kojima, M. I. Larkin, J. Merrin, B. Nachumi, Y. J. Uemura, Y. Maeno, Z. Q. Mao, Y. Mori, H. Nakamura, and M. Sigrist, Nature (London) **394**, 558 (1998).

[7] J. Xia, Y. Maeno, P. T. Beyersdorf, M. M. Fejer, and A. Kapitulnik, Phys. Rev. Lett. **97**, 167002 (2006).

[8] Y. Maeno, T. Ando, Y. Mori, E. Ohmichi, S. Ikeda, S. NishiZaki, and S. Nakatsuji, Phys. Rev. Lett. **81**, 3765 (1998).

[9] H. Kaneyasu, N. Hayashi, B. Gut, K. Makoshi, and M. Sigrist, J. Phys. Soc. Jpn. **79**, 104705 (2010).

[10] Z. Q. Mao, K. D. Nelson, R. Jin, Y. Liu, and Y. Maeno, Phys. Rev. Lett. **87**, 037003 (2001).

[11] M. Kawamura, H. Yaguchi, N. Kikugawa, Y. Maeno, and H. Takayanagi, J. Phys. Soc. Jpn. **74**, 531 (2005).

[12] S. Kashiwaya, H. Kashiwaya, H. Kambara, T. Furuta, H. Yaguchi, Y. Tanaka, and Y. Maeno, Phys. Rev. Lett. **107**, 077003 (2011).

[13] F. Kidwingira, J. D. Strand, D. J. Van Harlingen, and Y. Maeno, Science **314**, 1267 (2006).

[14] H. Kambara, S. Kashiwaya, H. Yaguchi, Y. Asano, Y. Tanaka, and Y. Maeno, Phys. Rev. Lett. **101**, 267003 (2008).

[15] M. S. Anwar, T. Nakamura, S. Yonezawa, M. Yakabe, R. Ishiguro, H. Takayanagi, and Y. Maeno, Sci. Rep. **3**, 2480 (2013).

[16] J. Hooper, Z. Q. Mao, K. D. Nelson, Y. Liu, M. Wada, and Y. Maeno, Phys. Rev. B **70**, 014510 (2004).

[17] C. Kallin and A. J. Berlinsky, J. Phys. Condens. Matter **21**, 164210 (2009).

[18] K. Saitoh, S. Kashiwaya, H. Kashiwaya, Y. Mawatari, Y. Asano, Y. Tanaka, and Y. Maeno, Phys. Rev. B **92**, 100504 (2015).

[19] P. J. Curran, S. J. Bending, W. M. Desoky, A. S. Gibbs, S. L. Lee, and A. P. Mackenzie, Phys. Rev. B **89**, 144504 (2014).

[20] D. J. Van Harlingen, Rev. Mod. Phys. **67**, 515 (1995).

[21] E. W. Fenton, Solid State Commun. **54**, 709 (1985).

[22] V. B. Geshkenbein and A. I. Larkin, Pis'ma Zh. Eksp. Teor. Fiz. **43**, 306 (1986) [JETP Lett. **43**, 395 (1986)].

[23] A. Millis, D. Rainer, and J. A. Sauls, Phys. Rev. B **38**, 4504 (1988).

[24] Y. Hasegawa, J. Phys. Soc. Jpn. **67**, 3699 (1998).

[25] R. Jin, Y. Liu, Z. Q. Mao, and Y. Maeno, Europhys. Lett. **51**, 341 (2000); Y. Liu, K. D. Nelson, Z. Q. Mao, R. Jin, and Y. Maeno, J. Low Temp. Phys. **131**, 1059 (2003).

[26] Y. Asano, Y. Tanaka, M. Sigrist, and S. Kashiwaya, Phys. Rev. B **67**, 184505 (2003); **71**, 214501 (2005).

[27] Y. Liu, New J. Phys. **12**, 075001 (2010).

[28] A. Sumiyama, T. Endo, Y. Oda, Y. Yoshida, A. Mukai, A. Ono, and Y. Onuki, Phys. C (Amsterdam, Neth.) **367**, 129 (2002).

[29] K. Saito, S. Kashiwaya, H. Kashiwaya, M. Koyanagi, Y. Mawatari, Y. Tanaka, and Y. Maeno, Appl. Phys. Exp. **5**, 113101 (2012).

[30] R. Jin, Yu. Zadorozhny, Y. Liu, D. G. Schlom, Y. Mori, and Y. Maeno, Phys. Rev. B **59**, 4433 (1999).

[31] M. Yamashiro, Y. Tanaka, and S. Kashiwaya, J. Phys. Soc. Jpn. **67**, 3364 (1998).

[32] C. Honerkamp and M. Sigrist, Prog. Theor. Phys. **100**, 53 (1998).

[33] T. Nakamura, R. Nakagawa, T. Yamagishi, T. Terashima, S. Yonezawa, M. Sigrist, and Y. Maeno, Phys. Rev. B **84**, 060512 (2011); T. Nakamura, T. Sumi, S. Yonezawa, T. Terashima, M. Sigrist, H. Kaneyasu, and Y. Maeno, J. Phys. Soc. Jpn. **81**, 064708 (2012).

[34] H. Kaneyasu and M. Sigrist, J. Phys. Soc. Jpn. **79**, 053706 (2010).

[35] S. B. Etter, H. Kaneyasu, M. Ossadnik, and M. Sigrist, Phys. Rev. B **90**, 024515 (2014).

[36] H. Kaneyasu, S. B. Etter, T. Sakai, and M. Sigrist, Phys. Rev. B **92**, 134515 (2015).

[37] Y. A. Ying, Y. Xin, B. W. Clouser, E. Hao, N. E. Staley, R. J. Myers, L. F. Allard, D. Fobes, T. Liu, Z. Q. Mao, and Y. Liu, Phys. Rev. Lett. **103**, 247004 (2009).

[38] K. D. Nelson, Z. Q. Mao, Y. Maeno, and Y. Liu, Science **306**, 1151 (2004).

[39] R. Ishiguro, M. Yakabe, T. Nakamura, E. Watanabe, D. Tsuya, H. Oosato, Y. Maeno, and H. Takayanagi, J. Phys. Conf. Ser. **400**, 022035 (2012).

[40] R. Ishiguro, T. Sakurai, M. Yakabe, T. Nakamura, S. Yonezawa, S. Kashiwaya, H. Takayanagi, and Y. Maeno, J. Phys. Conf. Ser. **568**, 022020 (2014).

[41] Y. Nago, R. Ishiguro, T. Sakurai, M. Yakabe, T. Nakamura, S. Yonezawa, S. Kashiwaya, H. Takayanagi, and Y. Maeno, J. Phys. Conf. Ser. **568**, 022031 (2014).

[42] R. Matzdorf, Z. Fang, Ismail, J. Zhang, T. Kimura, Y. Tokura, K. Terakura, and E. W. Plummer, Science **289**, 746 (2000).

[43] I. Bonalde, B. D. Yanoff, M. B. Salamon, D. J. Van Harlingen, E. M. E. Chia, Z. Q. Mao, and Y. Maeno, Phys. Rev. Lett. **85**, 4775 (2000).

[44] B. Chesca, R. Kleiner, and D. Koelle, in *The SQUID Handbook*, Vol. 1, *Fundamentals and Technology of SQUIDs and SQUID Systems*, edited by J. Clarke and A. I. Braginski (Wiley-VCH, Weinheim, 2004), Chap. 2.

[45] R. L. Fagaly *et al.*, in *Applied Superconductivity: Handbook on Devices and Applications*, edited by P. Seidel (Wiley-VCH, Weinheim, 2015), Vol. 2, Chap. 9.

[46] C. Granata and A. Vettoliere, Phys. Rep. **614**, 1 (2016).

[47] A. G. P. Troeman, S. H. W. van der Ploeg, E. Il'Ichev, H.-G. Meyer, A. A. Golubov, M. Yu. Kupriyanov, and H. Hilgenkamp, Phys. Rev. B **77**, 024509 (2008).

[48] M. Tinkham, *Introduction to Superconductivity*, 2nd ed. (Dover, New York, 2004), Chaps. 3 and 6.

[49] We found that the small modulation of I_c around 1.45 K is not quite a regular periodic one. That is why the data for ΔB_{SQ}

and B_0 around 1.45 K are omitted in Figs. 4 and 5(b). Such irregular signals might be due to the effects of the 3-K phase. Experimental results around 1.45 K and higher temperatures (3-K phase) will be discussed elsewhere.

[50] T. Golod, A. Rydh, and V. M. Krasnov, Phys. Rev. Lett. **104**, 227003 (2010).

[51] S. Tsuchiya, M. Matsuno, R. Ishiguro, H. Kashiwaya, S. Kashiwaya, S. Nomura, H. Takayanagi, and Y. Maeno, J. Phys. Soc. Jpn. **83**, 094715 (2014).

[52] Y. Nago, T. Shinozaki, S. Tsuchiya, R. Ishiguro, H. Kashiwaya, S. Kashiwaya, S. Nomura, K. Kono, H. Takayanagi, and Y. Maeno, J. Low Temp. Phys. **183**, 292 (2016).

[53] D. Sakuma, T. Shinozaki, Y. Nago, R. Ishiguro, S. Kashiwaya, S. Nomura, K. Kono, and H. Takayanagi, J. Low Temp. Phys. **183**, 300 (2016).